

Constraints on the phase transition of Early Dark Energy with the CMB anisotropies

Shintaro Hayashi ^a, Teppei Minoda ^b, Kiyotomo Ichiki ^{a,c}

^a*Department of Physics and Astrophysics, Nagoya University, Chikusa-ku, Nagoya, 464-8602, Japan*

^b*The University of Melbourne, School of Physics, Parkville, VIC 3010, Australia*

^c*Kobayashi-Maskawa Institute for the Origin of Particles and the Universe, Nagoya University, Chikusa-ku, Nagoya 464-8602, Japan*

Abstract

Early dark energy models have attracted attention in the context of the recent problem of the Hubble tension. Here we extend these models by taking into account the new density fluctuations generated by the dark energy decays around the recombination phase. We solve the evolution of the density perturbations in dark energy fluid generated at the phase transition of early dark energy as isocurvature perturbations. Assuming that the isocurvature mode is characterized by a power-law power spectrum and is uncorrelated with the standard adiabatic mode, we calculate the CMB angular power spectra and compare them to the Planck data using the Markov-Chain Monte Carlo method. As a result, we obtained the zero-consistent values of the EDE parameters and $H_0 = 67.47_{-1.00}^{+1.01} \text{ km s}^{-1} \text{ Mpc}^{-1}$ at 68% CL. This H_0 value is almost the same as the Planck+ Λ CDM value, $H_0 = 67.36 \pm 0.54 \text{ km s}^{-1} \text{ Mpc}^{-1}$, and there is still a $\sim 3\sigma$ tension between the CMB and Type Ia supernovae observation. Moreover, the amplitude of the spectra induced by the phase transition of the EDE is constrained to be less than one percent of that of the adiabatic mode. This is so small that such non-standard fluctuations cannot appear in the CMB angular spectra. In conclusion, we need to carefully examine different types of EDE models, and/or the combined data analysis, while the isocurvature fluctuations induced by our simplest EDE phase transition model do not explain the Hubble tension well.

1 Introduction

The Hubble constant H_0 is estimated by various observations [1–6]. Recently, there arises a discrepancy between values estimated from the early-time and late-time observations. As an early-time observation, the latest measurements of the cosmic microwave background (CMB) anisotropies by the Planck collaboration give $H_0 = 67.36 \pm 0.54 \text{ km s}^{-1}\text{Mpc}^{-1}$ by assuming the Λ CDM model [1]. On the other hand, the SH0ES Collaboration using Cepheids and Type Ia supernovae shows a higher value as $H_0 = 73.04 \pm 1.04 \text{ km s}^{-1}\text{Mpc}^{-1}$ [2]. The difference in estimated H_0 is called "Hubble tension" and some alternative theories beyond Λ CDM have been proposed to resolve the Hubble tension (including, for example, non-cold dark matter [7], dynamical dark energy [8], time-varying electron mass [9], and small-scale density fluctuations [10, 11]).

Early dark energy (EDE) is one of the ideas to solve the Hubble tension [12–17]. It is motivated by the string-axion, and behaves like the cosmological constant before the critical epoch $a < a_c$. After that, EDE starts to decay rapidly. This behavior plays an important role in the estimate of H_0 from measurements of the CMB anisotropies. CMB observations precisely determine the angular size of the sound horizon θ_s^* , which is the ratio between the sound horizon at the last scattering surface r_s^* and the comoving angular diameter distance to the last scattering surface d_A^* . Here, the cosmological constant-like behavior of EDE enhances the expansion rate of the universe before the recombination epoch, and it reduces the sound horizon r_s^* . Because θ_s^* must be kept to the observed value, decreasing r_s^* requires the angular diameter distance to be smaller and as a result, H_0 is estimated to be larger.

While many studies attempted to relieve the Hubble tension by using this enhancement of the expansion rate at early times with an EDE model, most of them considered only the impact of the EDE on the background evolution [18]. Of course, as far as the EDE behaves as the cosmological constant, it never generates the evolution of density perturbations. On the other hand, the density perturbations of EDE is expected to be generated through the gravitational interaction after the EDE starts to decay. Such EDE perturbations and their important role in the CMB constraints have already been studied and discussed intensively [19]. In addition to those perturbations, because the decay of EDE occurs stochastically at each horizon patch, the isocurvature perturbations could be generated by the phase transition of EDE on the analogy of the bubble nucleation due to the first-order phase transition [20–22]. This is what we aim to study in this work. In Refs. [19] and [15], the authors argued that such perturbations do not appear on the observational scale of the CMB due to "trigger dynamics" or multiple phase transitions. In this paper, we treat these isocurvature fluctuations phenomenologically in cosmological perturbation theory and test whether such fluctuations are actually not allowed to exist from CMB observations.

In this paper, we study the effect of the EDE on the CMB anisotropies including the effect of EDE perturbations. In Sec. 2, we introduce the impact of the EDE that has a phase transition before the recombination epoch on the background and perturbation

evolutions. We perform a Markov Chain Monte Carlo (MCMC) analysis to put an observational constraint on the model parameters of the EDE with phase transition and discuss how much the Hubble tension is resolved. In Sec. 3, we show the calculation results for the perturbation equations and the constraints from the MCMC analysis with the Planck CMB measurements. Finally, we discuss and conclude in Sec. 4.

2 Methods

2.1 Background effect of early dark energy

The sound horizon at the last scattering r_s^* and the comoving angular diameter distance to the last scattering surface d_A^* can be written as

$$r_s^* = \int_{z^*}^{\infty} \frac{dz}{H(z)} c_s(z), \quad (2.1)$$

and,

$$d_A^* = \int_0^{z^*} \frac{dz}{H(z)} = \int_0^{z^*} \frac{dz}{H_0 \sqrt{\Omega_{r0}(1+z)^4 + \Omega_{m0}(1+z)^3 + \Omega_{\Lambda 0}}}, \quad (2.2)$$

respectively, where z^* is the redshift at the last scattering surface and $c_s(z)$ is the sound speed of the baryon-photon fluid. Note that we have assumed the standard Λ CDM model in the second equality in Eq.(2.2). In the EDE model, one introduces an additional energy component (EDE) in the standard Λ CDM model, which contributes to the energy density of the universe before recombination. Therefore the EDE reduces r_s^* by increasing $H(z)$ when the Λ CDM parameters remain unchanged. Recent precise measurements of the CMB anisotropies have determined the angular size of the sound horizon,

$$\theta_s^* = \frac{r_s^*}{d_A^*}. \quad (2.3)$$

Since θ_s^* is tightly constrained by the Planck 2018 CMB data, θ_s^* must be kept, and therefore, decreasing r_s^* should make d_A^* smaller and H_0 larger.

Our EDE model is based on the phenomenological treatment of an axion-like field, which was introduced in Ref. [12]. In this model, the EDE is assumed to be a slow-roll scalar field in the early epoch and becomes free after the critical epoch $a > a_c$. Moreover, we assume the energy density of the EDE is converted to the dark radiation(DR) at $a > a_c$ and the equation of state parameter of DR, $w_{\text{DR}} = 1$. We simply assume the equation of state of EDE with the above behaviors as

$$w_{\text{EDE}} = \begin{cases} -1 & a < a_c \\ 1 & a \geq a_c \end{cases}. \quad (2.4)$$

The total energy density is the sum of the energy densities of the components in the standard model and EDE, and given by

$$\rho_{\text{tot}} = \rho_{\text{ACDM}} + \rho_{\text{EDE}}, \quad (2.5)$$

$$\rho_{\text{EDE}} = \rho_{\text{EDE}}(a_c) \left(\frac{a_c}{a} \right)^{3(1+w_{\text{EDE}})}. \quad (2.6)$$

Note that some recent studies have used models with a more realistic potential of the axion fields [18], and our EDE model is the basic and simplest one.

This is the basic idea of EDE, and there are some concrete models to realize this such as ultra-light axion models [18]. In Figure 1, we show the time evolution of energy densities of some components.

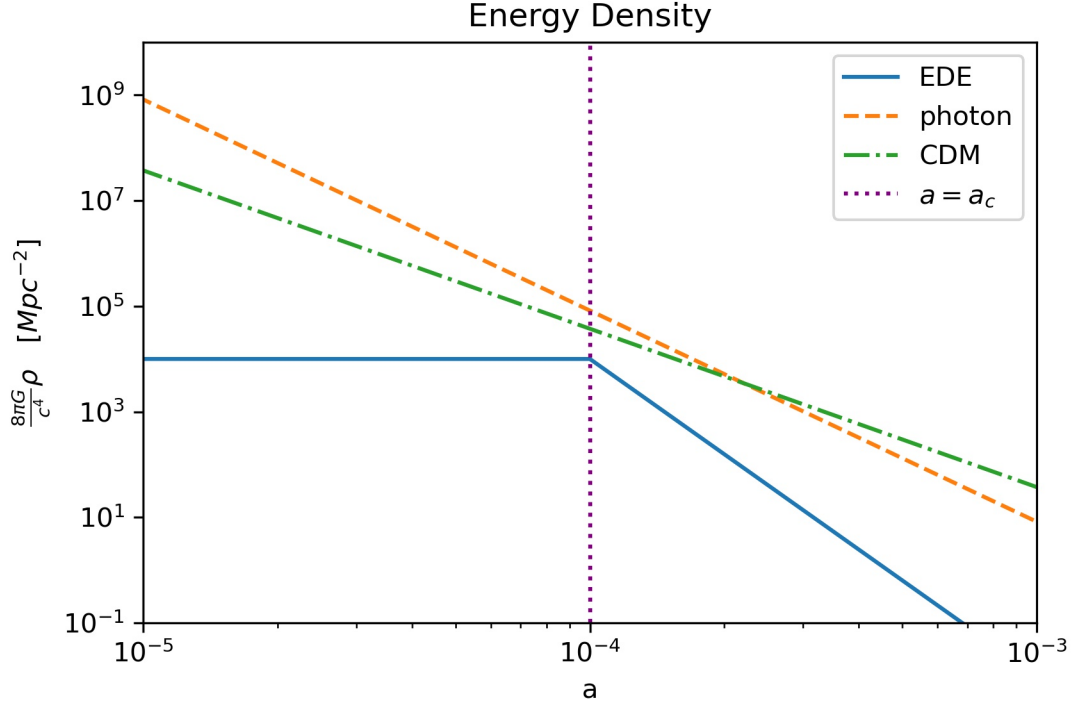


Figure 1: Time evolution of background energy densities of early dark energy (ρ_{EDE} ; blue solid line), photons (ρ_{γ} ; orange dashed line), and cold dark matter (ρ_{CDM} ; green dot-dashed line) as a function of scale factor a . For this particular plot, we choose $8\pi G\rho_{\text{EDE}}(a_c)/c^4 = 10^4$ [Mpc⁻²] and $a_c = 10^{-4}$, where a_c is the scale factor when the phase transition occurred.

2.2 Perturbation evolution of the EDE phase transition mode

In order to obtain the evolution of perturbations that were excited due to dark energy phase transition, we start at the perturbed energy-momentum conservation equations, $T^{\mu\nu}{}_{;\mu} = 0$, which lead to

$$\dot{\delta} + (1+w) \left(\theta + \frac{\dot{h}}{2} \right) + 3H \left(\frac{\delta P}{\delta \rho} - w \right) \delta = 0, \quad (2.7)$$

$$\dot{\theta} + H(1-3w) + \frac{\dot{w}}{1+w} \theta - \frac{\delta P / \delta \rho}{1+w} k^2 \delta = 0, \quad (2.8)$$

where δ and θ are defined as $\delta \equiv \delta \rho / \rho$ and $\theta \equiv ik^j v_j$. When treating dark energy as a fluid, one uses a sound speed c_s which is defined in the dark energy rest frame [23]. Moreover, we consider the source of the PT mode perturbation as something similar to an entropy perturbation, and therefore we have

$$\delta P = c_s^2 \delta \rho + 3H(1+w)(c_s^2 - w) \rho \frac{\theta}{k^2} + \rho S, \quad (2.9)$$

where S is the source term which arises during the EDE phase transition ($a_c \leq a \leq a_{\text{end}}$). By combining Eqs.(2.7)-(2.9), the EDE density perturbation δ_{EDE} and velocity perturbation θ_{EDE} in the synchronous gauge evolve according to the following equations,

$$\begin{aligned} \dot{\delta}_{\text{EDE}} + (1+w_{\text{EDE}}) \left(\theta_{\text{EDE}} + \frac{\dot{h}}{2} \right) + 3H(c_s^2 - w_{\text{EDE}}) \left[\delta_{\text{EDE}} + 3(1+w_{\text{EDE}}) \frac{\theta_{\text{EDE}}}{k^2} \right] \\ = \begin{cases} -3HS & (a_c \leq a \leq a_{\text{end}}) \\ 0 & (\text{others}) \end{cases}, \end{aligned} \quad (2.10)$$

$$\begin{aligned} \dot{\theta}_{\text{EDE}} + H(1-3c_s^2) \theta_{\text{EDE}} - \frac{k^2}{1+w_{\text{EDE}}} c_s^2 \delta_{\text{EDE}} \\ = \begin{cases} \frac{k^2}{1+w_{\text{EDE}}} S & (a_c \leq a \leq a_{\text{end}}) \\ 0 & (\text{others}) \end{cases}. \end{aligned} \quad (2.11)$$

The perturbations generated by the phase transition (hereafter, PT-mode) may have a k -dependence. We put the information about k -dependence in the initial power spectrum. We assume that the initial power spectrum of PT-mode has a power-law form as

$$\langle S(\vec{k}) S^*(\vec{k}') \rangle = (2\pi)^3 P_{\text{PT}}(k) \delta(\vec{k} - \vec{k}'), \quad (2.12)$$

where

$$\frac{k^3}{2\pi^2} P_{\text{PT}}(k) = A_{\text{amp}} \left(\frac{k}{k_{\text{PT}}} \right)^{n_{\text{PT}}-1}. \quad (2.13)$$

Here A_{amp} , k_{PT} and n_{PT} are the amplitude, pivot scale and spectral index of the PT-mode, respectively. As explained in the following section, A_{amp} is replaced with the rescaled parameter $A_{\text{PT}} \equiv \log_{10}(10^{10} A_{\text{amp}})$ in our MCMC analysis.

2.3 Implementation into CosmoMC

For the MCMC analysis, we have used the `CosmoMC` package [24, 25] and the Planck 2015 high- ℓ TT power spectra ($30 \leq \ell \leq 2508$) and the low- ℓ temperature and LFI polarization ($2 \leq \ell \leq 29$) as the data set. We have modified CAMB [26] to calculate the perturbation evolution and the CMB spectra made by PT. We have added 4 new parameters, a_c , a_{end} , $\rho_{\text{EDE}}(a_c)$ and A_{PT} into CAMB and they are the free parameters in the MCMC in addition to the standard six cosmological parameters. Here, A_{PT} is defined as $A_{\text{PT}} \equiv \log_{10}(10^{10} A_{\text{amp}})$ for convenience. Although we have also put n_{PT} into CAMB as a parameter, in the following analysis, it is not the free parameter and fixed to 4 in order to take into account that the phase transition occurred spatially at random and the perturbations have a white noise spectrum. We put the flat priors on the parameters and show them in Table 1. We use the same priors range for all our analysis. The MCMC sampling stops when the convergence reaches the Gelman and Rubin R condition [27] and we set $R - 1 < 0.01$ for all our analysis.

	Parameter	Priors
Λ CDM parameters	$\Omega_b h^2$	[0.05, 0.1]
	$\Omega_c h^2$	[0.001, 0.99]
	τ	[0.01, 0.8]
	$100\Theta_s$	[0.5, 10]
	n_s	[0.7, 1.2]
	$\log A_s$	[2, 5]
EDE parameters	$8\pi G\rho_{\text{EDE}}/c^4$	[0, 5000]
	a_c	[0.00001, 0.0003]
PT parameters	A_{PT}	[1.5, 7.5]
	a_{end}	[0.0004, 0.0006]

Table 1: The priors distribution on the parameters are shown.

3 Results and Discussion

3.1 Evolution of the density perturbation

We show the results of perturbation evolution of the PT-mode at some wavenumbers in Figure 2. We assumed the perturbation evolution of the PT-mode is independent of the adiabatic mode, and here we set the initial conditions for the adiabatic mode perturbations as zero, in order to simply illustrate the PT-mode perturbations. Therefore, it can be seen that there is no fluctuation until PT occurs and δ_{EDE} starts to oscillate when the source term appears at $a = a_c$ when PT happens. In the larger k -mode, the faster the EDE

density perturbation oscillates. The EDE perturbation gravitationally propagates to other perturbations. At first, the oscillation phase of density perturbation of other components is inverse of that of EDE. This is because the local expansion rate is faster and the energy densities of the other fluid components are lower where the EDE energy density is higher than the background. In the early universe, baryons are tightly coupled with photons, and the density perturbations of the baryon and photon before recombination evolve together. The CDM density perturbation is initially generated by that of the EDE gravitationally. Once it is generated, it grows up by its self-gravity.

The end of the PT period is shown as the vertical black line in Figure 2. Although we can see a small effect on the evolution of density perturbations from the end of the PT in the change of the oscillation center, it is clear that the gravitational growth and the acoustic oscillation of the perturbation dominate after PT happens.

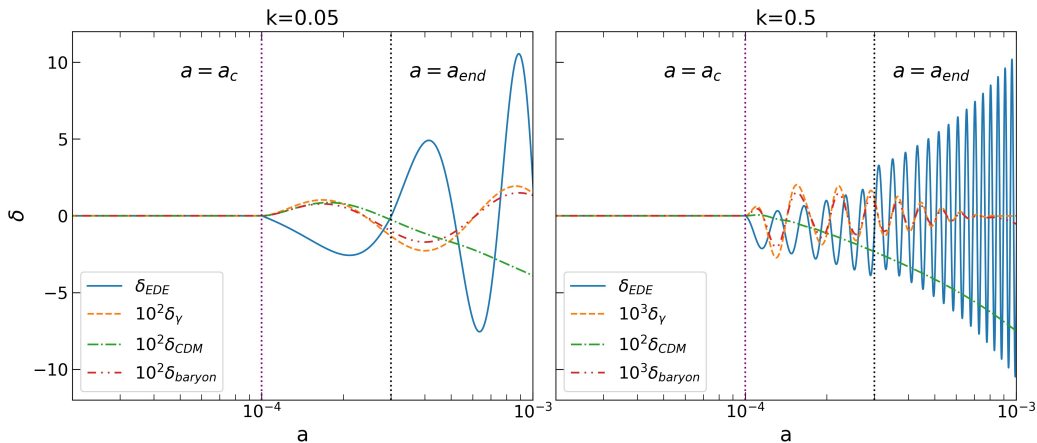


Figure 2: Time evolution of density perturbations of EDE (δ_{EDE} , solid), photons (δ_γ , dashed), cold dark matter (δ_{CDM} , dot-dashed), and baryons (δ_{baryon} , dotted), at wavenumber $k = 0.05$ [Mpc^{-1}] (left panel) and $k = 0.5$ [Mpc^{-1}] (right panel). The purple and black dashed vertical lines show the beginning and end of the PT. The perturbations are generated at $a = a_c$ and grow up after that. The oscillation center slightly changes at $a = a_{\text{end}}$, respectively. In this figure, the amplitudes of δ_γ , δ_{CDM} and δ_{baryon} are multiplied by a factor of 10^2 or 10^3 for clarity.

3.2 Power spectra of CMB anisotropies from the phase transition mode

We show the effect of the PT-mode perturbations on the CMB angular power spectrum C_ℓ^{PT} in Figure 3 and 4. In the left panel of Figure 3, we have chosen the initial energy densities of the EDE as $8\pi G\rho_{\text{EDE}}/c^4 = 10^4, 5 \times 10^4$ and 10^5 [Mpc^{-2}]. It can be seen that ρ_{EDE} only changes the amplitude of the spectra and the higher energy density of EDE

leads to the larger amplitude of spectra. We also show the angular power spectra with different phase transition times of the EDE a_c in the right panel of Figure 3. According to this figure, a_c does not only affect the amplitude but also changes the peak positions. The smaller a_c is, the earlier EDE decays and the lower is the ratio of the EDE energy density to the total energy density during the phase transition. Therefore, the amplitude of spectra becomes smaller due to the smaller early-ISW effect. The parameter a_c also controls the beginning of the phase transition, and the smaller a_c shifts the peak positions to the larger scale. These parameters affect the background level as we explained in Section 2, and thus they also affect the adiabatic mode perturbations. On the other hand, a_{end} does not contribute to the background evolution. Moreover, as we saw previously, the growth of the EDE density perturbation is dominated by its self-gravity after the source term appears at a_c . Therefore, the effects of a_{end} on the perturbation evolution are also small. Actually, as shown in Figure 4, the difference between CMB angular power spectra with $a_{\text{end}} = 3 \times 10^{-4}$ and 8×10^{-4} is suppressed within 20 percent.

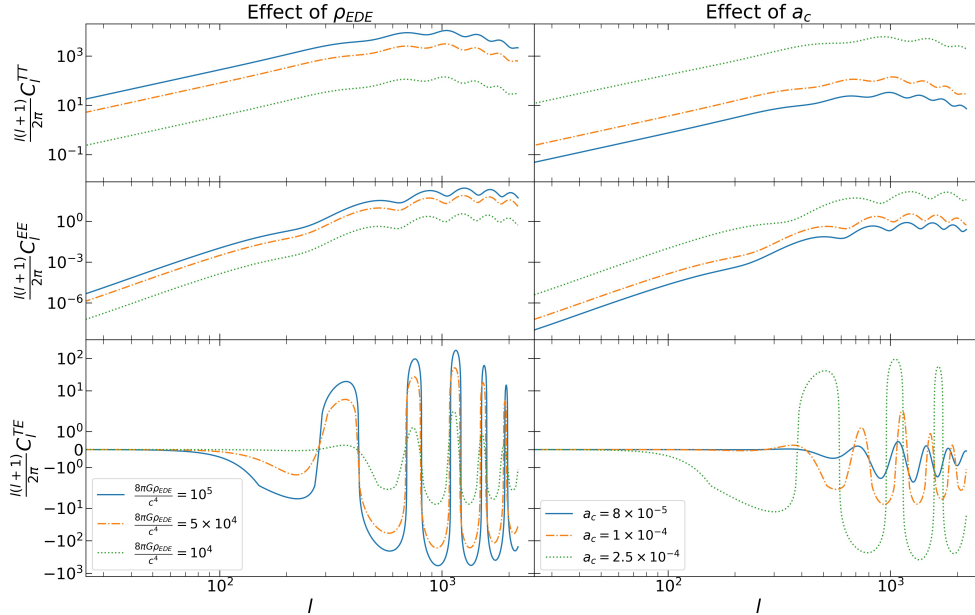


Figure 3: The CMB angular power spectra of the PT-mode. We only show the multipole range of $l \geq 25$ because the spectra simply decay with a power-law at $l \leq 25$. In the left panel, the EDE energy density before the phase transition is taken as $8\pi G\rho_{\text{EDE}}/c^4$, 10^4 , 5×10^4 and 10^5 [Mpc^{-2}] with $a_c = \text{fixed to } 1 \times 10^{-4}$. In the right panel, we set $8\pi G\rho_{\text{EDE}}/c^4 = 10^4[\text{Mpc}^{-2}]$ and vary a_c as 8×10^{-5} , 10^{-4} and 2.5×10^{-4} . In both cases, the other EDE and PT related parameters are fixed to $a_{\text{end}} = 3 \times 10^{-4}$ and $A_{\text{PT}} = 4$.

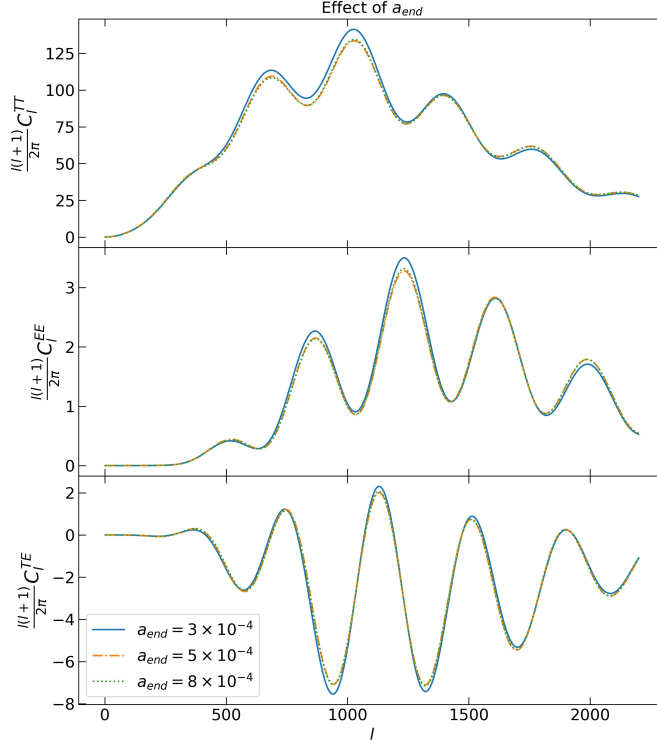


Figure 4: We have changed a_{end} to 3×10^{-4} , 5×10^{-4} and 8×10^{-4} . The other parameters are fixed to $8\pi G\rho_{\text{EDE}}/c^4 = 10^4[\text{Mpc}^{-2}]$, $a_c = 1 \times 10^{-4}$ and $A_{\text{PT}} = 4$. The effect of a_{end} is limited to only the slightly changes of the peak amplitude.

3.3 Constraints on EDE model with MCMC

We plot the results of the MCMC analysis in Figure 5. The blue contours show the constraints in the ΛCDM model, and the grey contours marked as “EDE+PT” indicate the constraints in the EDE model with the phase transition. We also show the case of the EDE model without PT-mode indicated by the red contour labeled “EDE” to compare the results of our EDE model with those of the simple EDE model used in previous studies [14, 28, 29]. We show the best-fitted values and constraints with 68% confidence level in Table 2.

First, we discuss the constraints on the EDE parameters. We found that smaller values for ρ_{EDE} , a_c , and A_{PT} are favored because the larger values of them affect the CMB power spectra as discussed in the previous section. As a result, all parameters of the EDE are zero-consistent, and we obtained only the upper limits on ρ_{EDE} , a_c , and A_{PT} in Table 2. We also found no significant difference between the constraints in the EDE model with

Parameter	Λ CDM	EDE + PT	EDE
$100\Omega_b h^2$	2.223 (2.223) $^{+0.023}_{-0.023}$	2.227 (2.236) $^{+0.024}_{-0.025}$	2.228 (2.223) $^{+0.024}_{-0.027}$
$\Omega_c h^2$	0.1198 (0.1199) $^{+0.0022}_{-0.0022}$	0.1120 (0.1225) $^{+0.0022}_{-0.0026}$	0.1202 (0.1229) $^{+0.0022}_{-0.0027}$
r_s^*	144.60 (144.57) $^{+0.50}_{-0.49}$	144.44 (143.24) $^{+0.69}_{-0.48}$	144.33 (143.32) $^{+0.78}_{-0.48}$
H_0	67.32 (67.24) $^{+0.96}_{-1.04}$	67.47 (67.91) $^{+1.01}_{-1.00}$	67.46 (67.24) $^{+1.01}_{-1.01}$
$8\pi G\rho_{\text{EDE}}(a_c)/c^4$	-	1.91 (0.39) $^{+0.78} \times 10^3$	1.78 (0.34) $^{+0.66} \times 10^3$
a_c	-	8.36 (22.175) $^{+0.71} \times 10^{-5}$	9.53 (21.74) $^{+1.57} \times 10^{-5}$
A_{PT}	-	3.63 (3.33) $^{+0.76}$	-
a_{end}	-	5.00 (4.17) $^{+1.00}_{-1.00} \times 10^{-4}$	-
χ^2 (CMB)	11274.69 (11263.41)	11274.56 (11261.19)	11274.88 (11260.16)

Table 2: Mean values and 68% confidence intervals for some cosmological parameters in each model. The best-fit values are shown in the parentheses.

and without the phase transition. This is because A_{PT} is constrained below 4.39 at the 68% confidence level and this value is so small that the EDE PT-mode does not appear in the CMB spectra. We show the CMB angular spectra induced by the phase transition C_ℓ^{PT} and the total spectra C_ℓ^{total} in Figure 6. In this case, we fix the model parameters to the best-fit values in Table 2. In fact, the amplitude of C_ℓ^{PT} is more than two orders of magnitude smaller than the amplitude of C_ℓ^{total} , so only small contributions of EDE PT-mode are allowed.

For the end of the phase transition, we obtained $a_{\text{end}} = 5.00^{+1.00}_{-1.00} \times 10^{-4}$. This is the same range as the input prior. As we showed in Figure 4 and discussed in section 3.2, the effect of a_{end} on the CMB power spectra is small. Therefore, a_{end} is not constrained by the Planck data.

As mentioned in Sections 1 and 2, an important motivation to introduce the EDE is to resolve the Hubble tension. However, our analysis shows that the constraints on the standard cosmological parameters including H_0 do not change significantly in the EDE models and the Λ CDM model. The least χ^2 values for the EDE models are not improved so much while the number of model parameters is increased by four (“EDE+PT”) and by two (“EDE”). For further discussion on resolving the Hubble tension, we plot the two-dimensional constraint on the sound horizon at the recombination r_s^* and the Hubble constant H_0 in the left panel of Figure 7. This shows that although the constraints in the EDE models are slightly relaxed in the direction of smaller r_s^* and larger H_0 , it is difficult to fully solve the Hubble tension. Then we introduce a new parameter to evaluate the resolution degree of the Hubble tension, f_{EDE} , which is defined by the fraction of the EDE energy density to the total energy density. For the successful EDE scenario to resolve the H_0 tension, it is said that f_{EDE} needs to exceed 0.1 around the matter-radiation equality [30, 31]. However, f_{EDE} reaches around 0.05 even at the peak as shown in the right panel of Figure 7. Therefore, the EDE does not give the enough change in the value

of the Hubble parameter.

4 Summary

In this paper, we phenomenologically investigated the effects on CMB anisotropies at background and perturbation levels of the EDE model with phase transition. We then provided observational constraints from the Planck data. The phase transition of the EDE should occur at different epochs for different horizon patches, producing the “PT-mode” cosmological perturbations, which are independent of adiabatic ones predicted by inflationary mechanisms. We calculated the time evolution of the PT-mode perturbations and the resultant CMB angular power spectrum for the first time, and constrained the parameters of Λ CDM cosmology and the EDE model.

We modified the Boltzmann code CAMB by adding source terms into the perturbed equations for the EDE fluid to introduce the PT-mode. Here we used a power-law type initial power spectrum to determine the PT-mode source terms. For simplicity, we considered a white noise-like initial power spectrum for the PT-mode, and we set $n_{\text{PT}} = 4$. We performed the MCMC analysis by using Planck 2015 data, based on our modified CAMB code. As a result, the amplitude of the PT-mode perturbation was limited to less than 10^{-4} at 95% confidence level. This is so small that the effect does not appear in the CMB angular spectra. Thus, we conclude that the simple PT-mode EDE model cannot solve the Hubble tension.

Finally, we discuss two points of the possible extensions of this work. First, the results may change if we combine other data, e.g., Type Ia supernovae and/or the baryon acoustic oscillations in the galaxy surveys, although we have used only the CMB data in this paper. In particular, it is known that the EDE models show a larger value of H_0 when including the SH0ES data [30]. Second, there is uncertainty about the equation of state parameter after the EDE decays, w_{DR} . We assume $w_{\text{DR}} = 1$ in this paper. However, in Ref. [19], the equation of state parameter of the dark radiation is suggested in the range of $1/3 < w_{\text{DR}} < 1$ and preferred to be around 0.7 as the results of their analysis. Our choice for the equation of state parameter leads the fastest decay of EDE. Therefore the contribution of EDE becomes minimal. The lower equation of state parameter could lead the larger effect of EDE. It is worthwhile to investigate such further MCMC analyses by combining different observations and assuming more complicated EDE models. However, because it is beyond the scope of this paper, we put them as future works.

5 Acknowledgement

We would like to thank L. Herold and S. Yokoyama for useful discussions. This work is supported in part by JSPS Overseas Research Fellowship (TM), and the JSPS grant numbers 18K03616, 17H01110 and JST AIP Acceleration Research Grant JP20317829 and JST FOREST Program JPMJFR20352935 (KI).

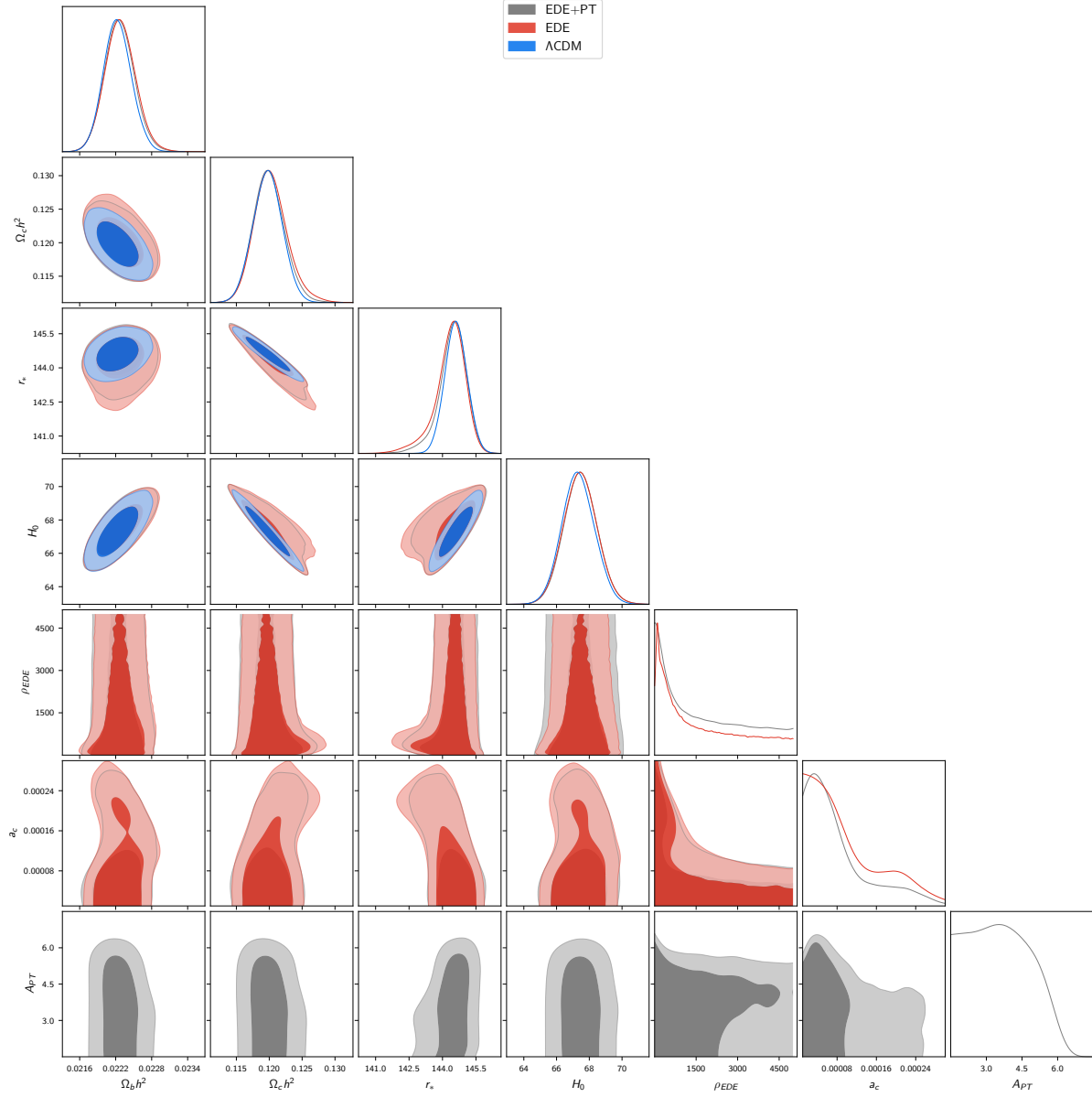


Figure 5: 68% and 95% confidence regions obtained from the MCMC analysis. The blue, grey and red contour shows the Λ CDM, EDE+PT and EDE model.

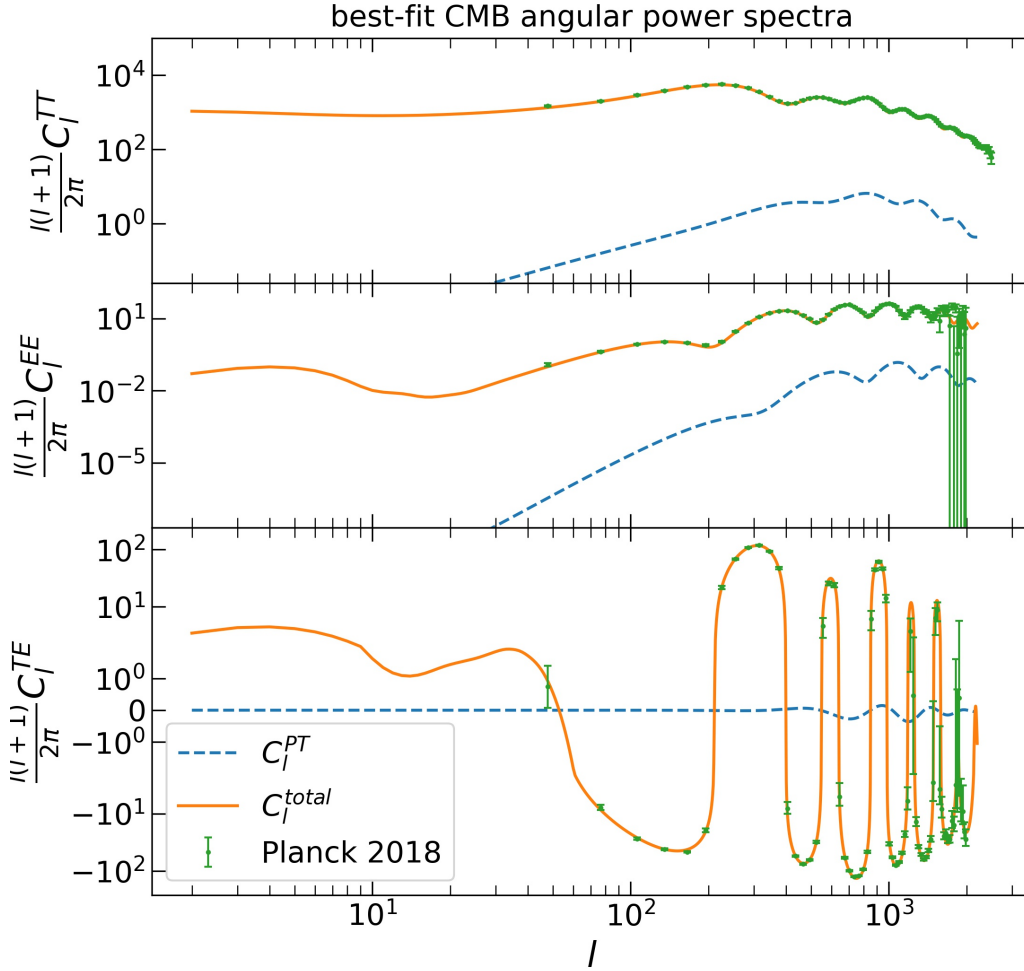


Figure 6: CMB angular power spectra of temperature and E-mode auto-correlations C_ℓ^{TT} (top) and C_ℓ^{EE} (middle), and temperature E-mode cross-correlation C_ℓ^{TE} (bottom) that arise from the EDE PT-mode. The model parameters are fixed to the best-fit values which are shown in Table 2. The TT and EE spectra of the PT mode (blue dashed lines) simply decay in the power-law form at the lower l region. Therefore we only show the ranges of $\frac{\ell(\ell+1)}{2\pi}C_\ell^{TT} \geq 2.5 \times 10^{-2}$ and $\frac{\ell(\ell+1)}{2\pi}C_\ell^{EE} \geq 2 \times 10^{-8}$ in those panels.

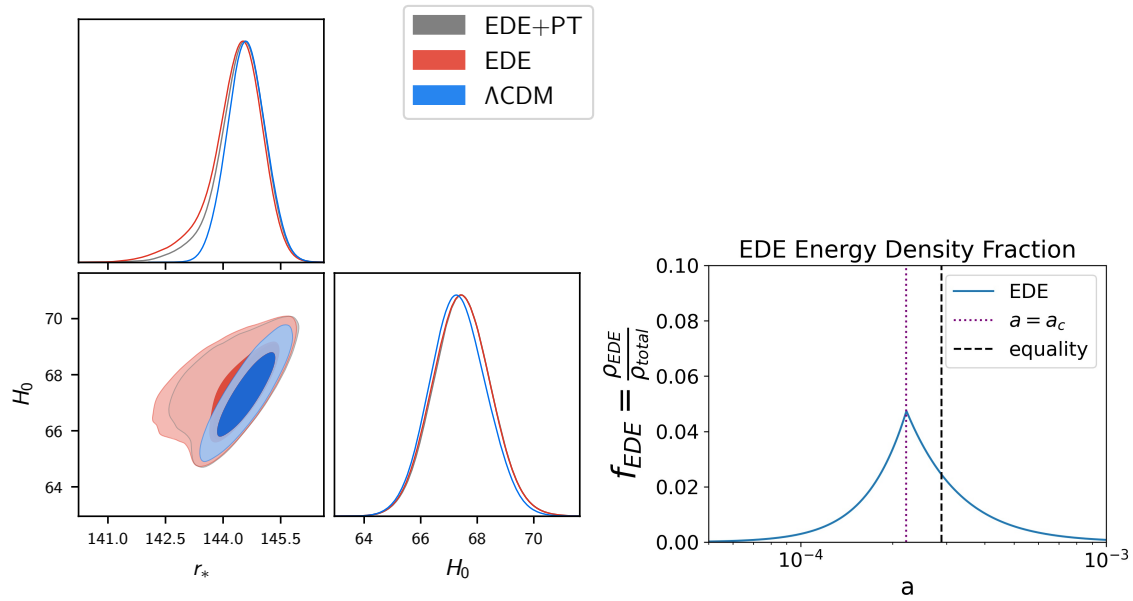


Figure 7: Left: Comparison between the constraints on H_0 and r_* obtained in the standard Λ CDM model and the EDE model with the PT-mode. Although our EDE model slightly reduces the Hubble tension, the difference in estimated mean values of H_0 is within much smaller range than 68% errors. Right: Time evolution of f_{EDE} , which is the ratio of the EDE energy density to the total energy density. In this calculation we used the best-fit values of ρ_{EDE} and a_c in the second column (EDE+PT) of Table 2. The black dashed line shows the matter-radiation equality.

References

- [1] **Planck** Collaboration, N. Aghanim et al., *Planck 2018 results. VI. Cosmological parameters*, *Astron. Astrophys.* **641** (2020) A6, [[arXiv:1807.06209](#)]. [Erratum: *Astron. Astrophys.* 652, C4 (2021)].
- [2] A. G. Riess et al., *A Comprehensive Measurement of the Local Value of the Hubble Constant with 1 km/s/Mpc Uncertainty from the Hubble Space Telescope and the SH0ES Team*, [arXiv:2112.04510](#).
- [3] V. Bonvin, F. Courbin, S. H. Suyu, P. J. Marshall, C. E. Rusu, D. Sluse, M. Tewes, K. C. Wong, T. Collett, C. D. Fassnacht, T. Treu, M. W. Auger, S. Hilbert, L. V. E. Koopmans, G. Meylan, N. Rumbaugh, A. Sonnenfeld, and C. Spiniello, *H0LiCOW - V. New COSMOGRAIL time delays of HE 0435-1223: H_0 to 3.8 per cent precision from strong lensing in a flat Λ CDM model*, *MNRAS* **465** (Mar., 2017) 4914–4930, [[arXiv:1607.01790](#)].
- [4] G. E. Addison, *High H_0 Values from CMB E-mode Data: A Clue for Resolving the Hubble Tension?*, *ApJ* **912** (May, 2021) L1, [[arXiv:2102.00028](#)].
- [5] S. Mukherjee, G. Lavaux, F. R. Bouchet, J. Jasche, B. D. Wandelt, S. Nissanke, F. Leclercq, and K. Hotokezaka, *Velocity correction for Hubble constant measurements from standard sirens*, *A&A* **646** (Feb., 2021) A65, [[arXiv:1909.08627](#)].
- [6] J.-J. Wei and F. Melia, *Exploring the Hubble Tension and Spatial Curvature from the Ages of Old Astrophysical Objects*, *ApJ* **928** (Apr., 2022) 165, [[arXiv:2202.07865](#)].
- [7] E. Elizalde, J. Gluza, and M. Khurshudyan, *An approach to cold dark matter deviation and the H_0 tension problem by using machine learning*, *arXiv e-prints* (Apr., 2021) arXiv:2104.01077, [[arXiv:2104.01077](#)].
- [8] S. Vagnozzi, *New physics in light of the H_0 tension: An alternative view*, *Phys. Rev. D* **102** (July, 2020) 023518, [[arXiv:1907.07569](#)].
- [9] T. Sekiguchi and T. Takahashi, *Early recombination as a solution to the H_0 tension*, *Phys. Rev. D* **103** (Apr., 2021) 083507, [[arXiv:2007.03381](#)].
- [10] K. Jedamzik and L. Pogosian, *Relieving the Hubble Tension with Primordial Magnetic Fields*, *Phys. Rev. Lett.* **125** (Oct., 2020) 181302, [[arXiv:2004.09487](#)].
- [11] M. Rashkovetskyi, J. B. Muñoz, D. J. Eisenstein, and C. Dvorkin, *Small-scale clumping at recombination and the Hubble tension*, *Phys. Rev. D* **104** (Nov., 2021) 103517, [[arXiv:2108.02747](#)].

- [12] T. Karwal and M. Kamionkowski, *Dark energy at early times, the Hubble parameter, and the string axiverse*, Phys. Rev. D **94** (Nov., 2016) 103523, [[arXiv:1608.01309](#)].
- [13] E. Mörtzell and S. Dhawan, *Does the Hubble constant tension call for new physics?*, J. Cosmology Astropart. Phys. **2018** (Sept., 2018) 025, [[arXiv:1801.07260](#)].
- [14] V. Poulin, T. L. Smith, T. Karwal, and M. Kamionkowski, *Early Dark Energy can Resolve the Hubble Tension*, Phys. Rev. Lett. **122** (June, 2019) 221301, [[arXiv:1811.04083](#)].
- [15] K. Freese and M. W. Winkler, *Chain early dark energy: A Proposal for solving the Hubble tension and explaining today's dark energy*, Phys. Rev. D **104** (Oct., 2021) 083533, [[arXiv:2102.13655](#)].
- [16] H. Moshafi, H. Firouzjahi, and A. Talebian, *Multiple transitions in vacuum dark energy and H_0 tension*, *arXiv e-prints* (Aug., 2022) arXiv:2208.05583, [[arXiv:2208.05583](#)].
- [17] K. Rezazadeh, A. Ashoorioon, and D. Grin, *Cascading Dark Energy*, *arXiv e-prints* (Aug., 2022) arXiv:2208.07631, [[arXiv:2208.07631](#)].
- [18] T. L. Smith, V. Poulin, and M. A. Amin, *Oscillating scalar fields and the Hubble tension: A resolution with novel signatures*, Phys. Rev. D **101** (Mar., 2020) 063523, [[arXiv:1908.06995](#)].
- [19] F. Niedermann and M. S. Sloth, *Resolving the Hubble tension with new early dark energy*, Phys. Rev. D **102** (Sept., 2020) 063527, [[arXiv:2006.06686](#)].
- [20] S. Coleman and F. de Luccia, *Gravitational effects on and of vacuum decay*, Phys. Rev. D **21** (June, 1980) 3305–3315.
- [21] A. H. Guth and E. J. Weinberg, *Could the universe have recovered from a slow first-order phase transition?*, *Nuclear Physics B* **212** (Feb., 1983) 321–364.
- [22] M. S. Turner, E. J. Weinberg, and L. M. Widrow, *Bubble nucleation in first-order inflation and other cosmological phase transitions*, Phys. Rev. D **46** (Sept., 1992) 2384–2403.
- [23] R. Bean and O. Doré, *Probing dark energy perturbations: The dark energy equation of state and speed of sound as measured by WMAP*, Phys. Rev. D **69** (Apr., 2004) 083503, [[astro-ph/0307100](#)].
- [24] A. Lewis, *Efficient sampling of fast and slow cosmological parameters*, Phys. Rev. D **87** (2013) 103529, [[arXiv:1304.4473](#)].
- [25] A. Lewis and S. Bridle, *Cosmological parameters from CMB and other data: A Monte Carlo approach*, Phys. Rev. D **66** (2002) 103511, [[astro-ph/0205436](#)].

- [26] A. Lewis, A. Challinor, and A. Lasenby, *Efficient computation of CMB anisotropies in closed FRW models*, ApJ **538** (2000) 473–476, [[astro-ph/9911177](#)].
- [27] A. Gelman and D. B. Rubin, *Inference from Iterative Simulation Using Multiple Sequences*, *Statistical Science* **7** (1992), no. 4 457 – 472.
- [28] L. Herold, E. G. M. Ferreira, and E. Komatsu, *New Constraint on Early Dark Energy from Planck and BOSS Data Using the Profile Likelihood*, ApJ **929** (Apr., 2022) L16, [[arXiv:2112.12140](#)].
- [29] J. S. Cruz, F. Niedermann, and M. S. Sloth, *A grounded perspective on New Early Dark Energy using ACT, SPT, and BICEP/Keck*, *arXiv e-prints* (Sept., 2022) arXiv:2209.02708, [[arXiv:2209.02708](#)].
- [30] J. C. Hill, E. McDonough, M. W. Toomey, and S. Alexander, *Early dark energy does not restore cosmological concordance*, Phys. Rev. D **102** (Aug., 2020) 043507, [[arXiv:2003.07355](#)].
- [31] M. M. Ivanov, E. McDonough, J. C. Hill, M. Simonović, M. W. Toomey, S. Alexander, and M. Zaldarriaga, *Constraining early dark energy with large-scale structure*, Phys. Rev. D **102** (Nov., 2020) 103502, [[arXiv:2006.11235](#)].